Biophysical Chemistry 168–169 (2012) 60–66

Contents lists available at SciVerse ScienceDirect

Biophysical Chemistry

journal homepage: http://www.elsevier.com/locate/biophyschem

Molecular mechanism of the interactions between inhibitory tripeptides and angiotensin-converting enzyme

Min Zhou [a], Kun Du [a], Peijun Ji [b], Wei Feng [a,*]

[a] Department of Biochemical Engineering, Beijing University of Chemical Technology, Beijing, China
[b] Department of Chemical Engineering, Beijing University of Chemical Technology, Beijing, China

HIGHLIGHTS

► MD simulations have identified a hydrophobic subsite in the active site of cACE.
► The interactions of the side chains of the tripeptides with the hydrophobic residues determine the binding positions of the tripeptides.
► This work presents the molecular mechanism of the interactions between the inhibitory tripeptides and ACE.

GRAPHICAL ABSTRACT

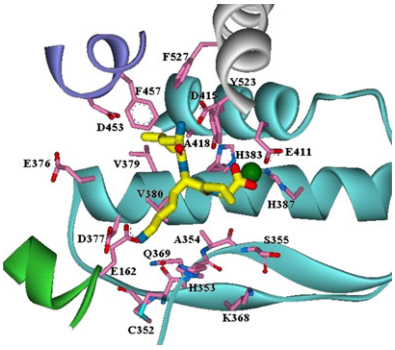

ARTICLE INFO

Article history:
Received 5 April 2012
Received in revised form 13 May 2012
Accepted 19 May 2012
Available online 23 May 2012

Keywords:
Angiotensin-converting enzyme
Tripeptide
Molecular dynamics simulation

ABSTRACT

Angiotensin I-converting enzyme (ACE) is a key therapeutic target for combating hypertension and related cardiovascular diseases. ACE inhibitory peptides offer the prospect of enhanced potency, high specificity, and no or low side effect. The ACE inhibitory tripeptides LKP and IKP differ from each other by one amino acid but their inhibitory potencies for ACE differ significantly. To uncover the molecular mechanism underlying this phenomenon, we have investigated the tripeptide/ACE complexes through molecular dynamics simulations coupled with quantum mechanical simulations. Comparative structural analysis has identified a hydrophobic subsite in the active site of cACE comprising hydrophobic residues Val379, Val380, Phe457, Phe527, and Ala418. The interactions of the side chains of Leu and Ile with the hydrophobic residues determine the binding positions of N-terminal residues of the tripeptides, that influence the interaction of the residues of tripeptides with the active site of cACE. This work presents the molecular mechanism of the interactions between the inhibitory tripeptides and ACE, and deciphers the structural basis for the high affinity LKP inhibition of ACE.

1. Introduction

Angiotensin I-converting enzyme (ACE) is a zinc metallopeptidase that can catalyze the proteolysis angiotensin I to the vasopressor angiotensin II, which is a potent vasoconstrictor, and inactivate bradykinin, which is a peptide that causes blood vessels to enlarge [1–3]. ACE exists as two isoforms: somatic ACE (sACE), comprised of two homologous N- and C-domains (cACE and nACE), and testis ACE (tACE) which has a single active domain [4,5]. ACE is a key therapeutic target for combating hypertension and related cardiovascular diseases [6]. Toward this end, much of the efforts have been focused on library search for and structure-based rational design of inhibitors that target ACE [7,8].

Synthetic ACE inhibitors, such as captopril, lisinopril, enalapril and fosinopril, are used as pharmaceuticals to treat hypertension, congestive

* Corresponding author at: Department of Biochemical Engineering, Beijing University of Chemical Technology, Beijing, China. Tel.: +86 10 64446249; fax: +86 10 64446249.
E-mail address: fengwei@mail.buct.edu.cn (W. Feng).

0301-4622/$ – see front matter © 2012 Elsevier B.V. All rights reserved.
doi:10.1016/j.bpc.2012.05.002

heart failure, and myocardial infarction [9]. However, these synthetic ACE inhibitors are known to have strong side effects, such as cough, skin rashes, and angioedema [10,11]. In recent years, inhibitory active peptides derived from the food protein have gained a lot of interest [11–16], because they have not shown these side effects yet [13]. ACE inhibitory peptides have been discovered in various food sources such as milk [11,13], pea [12], potato [14], and chicken meat [16]. Compared with synthetic inhibitors, peptides are capable of binding and antagonizing target proteins, often with high affinity and unsurpassed specificity [17].

Tripeptides have been shown to have inhibitory potency for ACE [18]. Some tripeptide exhibits much higher inhibitory potency than others. LKP, for example, has an IC_{50} of 0.32 μM while the IC_{50} value of IKP is 1.60 μM [18]. The inhibitory potency of LKP is 5-fold that of IKP. The superior inhibitory potency of LKP over IKP was surprising, partly because the tripeptide IKP differs from LKP by one amino acid, and Leu and Ile are isomeric amino acid residues. Unfortunately, the mechanism behind the experimental result was not provided. More insight into the inhibitory mechanisms may hold the key to further improvements in the design of ACE inhibitors.

As a complement to experiment in the study of ACE inhibitors, molecular simulation offers unique possibilities for investigating molecular-level phenomena that are difficult to probe experimentally [19–21]. These studies include the interactions of ACE with gonadotropin-releasing hormone by using molecular simulations [19]; molecular docking study for dual ACE/neutral endopeptidase inhibitors to investigate the molecular environment of the catalytic sites and the specific interactions between the inhibitors and amino acid residues [20]; the binding patterns of inhibitors of ACE [21].

Potent peptide inhibitors against ACE are needed as useful templates for structure-based rational design of different classes of ACE inhibitors for potential therapeutic use. Here, tripeptide/ACE systems are investigated. Based on quantum mechanics (QM) geometry optimization, a parameterization for the zinc ion and coordinating atoms is provided. Molecular dynamic simulations are performed to study the molecular mechanism of the interactions of inhibitory tripeptides LKP and IKP with ACE. The simulations interpret that, compared to LKP, IKP is much less inhibitory toward ACE.

2. Materials and methods

2.1. Structure preparation

The crystal structure of ACE bound with lisinopril was taken from Protein Data Bank at Brookhaven. The entry codes are 1O86 and 2C6N for the C-domain (tACE, which is identical to the C domain of sACE) and N-domain of sACE, respectively. Fig. S1 shows the inhibitor lisinopril in the active site. Except zinc and chloride ions, all heteroatoms were removed. Swiss-PdbViewer [22] was used to add the missing atoms and hydrogen atoms. The program H++ was used to predict the protonation state of ionizable groups at pH 7.0 by utilizing a continuum electrostatic model with the Poisson–Boltzmann method [23]. The added atoms were subjected to 500 rounds of energy minimization with steepest descent gradients using the GROMACS software package (version 4.05) [24] using the GROMOS-96 force field [25–28], while all other atoms were kept fixed [19]. The size of the system is listed in Table 1.

2.2. Docking of the inhibitors

The AutoDock 4.2 package was used for docking simulation [29], the visual inspection of the docking results was done using AutoDock-Tools. For the zinc and chloride ions, formal charges and van der Waals parameters from GROMOS 96 force field were assigned, and Kollman partial charges were assigned to all protein atoms. The maps for each domain of ACE centered at the zinc-binding site were calculated using AutoGrid with $40\times40\times40$ grid points of 0.375 Å spacing. The Lamarckian genetic algorithm was used, and the following AutoDock 4.2 parameters are selected: a population size of 150 individuals; a maximum number of 2.5×10^6 energy evaluations; a maximum number of 27,000 generations; an elitism value of 1; a mutation rate of 0.02; and a crossover rate of 0.80 [19]. For all the calculations, 250 docking rounds were performed with step sizes of 0.2 Å for translations and 5° for orientations and torsions. Docked conformations were clustered using a tolerance of 1.5 Å root mean square deviation. The predicted binding energy from the dockings provided a ranking of the docked conformations. The zinc coordination sphere in native ACE comprises His383/361, His387/365, and Glu411/389 (C-/N-domain numbering) [19]. Many inhibitors have been synthesized, and they differ in the nature of their zinc-binding ligands and other interaction groups. Captopril, for example, coordinates strongly the zinc atom in the active site of ACE by its sulfhydryl group [30], while enalaprilat and lisinopril contain a carboxylate group for coordinating the zinc atom [31]. In this work, the results of top-ranked binding modes indicate that the inhibitors LKP and IKP coordinate the zinc in the active site of ACE by their carboxylate groups. The docking results are used for the quantum mechanics (QM) and molecular dynamics (MD) simulations in the following sections.

Table 1
The size of the system.

System	No. of residues	Water	Total atoms
C-domain/LKP	574	20,221	66,717
C-domain/IKP	574	20,228	66,738
N-domain/LKP	612	21,668	71,481
N-domain/IKP	612	21,671	71,490

2.3. QM geometry optimization and zinc force field parameter

Due to the promiscuous ability of zinc to assume a variety of coordination states, zinc catalytic centers have long been a challenge for molecular modeling. Both nonbonded models [32–34] and bonded models [19,35–38] are suggested for the parameterization of zinc. In nonbonded approach [32–34], optimized electrostatics and van der Waals terms are used to enforce the correct coordination geometry. The bonded models utilize the bond terms including bond stretching, angle bending, and torsional terms [19,36–38]. These approaches require "freezing" a specific zinc coordination and a predefined valence of the coordinating metal.

Here, the bonded approach is adopted with explicit bonds between the zinc and its coordinating atoms. A model of the active site (Fig. 1) was extracted from the high-resolution crystal structure of tACE. The QM method was used to handle the zinc–ligand charge transfer, inter atom distances, and angles upon binding to the zinc. To reduce the convergence time for geometry optimization, the complex structure predicted by the best docking score was subjected to energy minimization using the steepest descent method. The model of the active site structure shown in Fig. 1 is used for the geometric optimization and the calculation of the zinc–inhibitor charge transfer. In this model, the zinc-binding motif was retained, except that Met was truncated into Gly and Glu411 into butyrate [19].

The docking of the two tripeptides with N- and C-domains was done independently. And then the geometric optimization for the ACE catalytic site was performed separately. The geometric optimization for the ACE catalytic site (Fig. 1) was performed with the Gaussian 03 package using the B3LYP method and 6-31G* basis set [39]. When performing MD simulations, the distances of Zn–Pro O1 were set to the values determined by the QM geometric optimization.

The calculated electrostatic potential was fitted with the RESP (restrained electrostatic potential) program [40] to handle the zinc–inhibitor charge transfer between the zinc and its coordinating atoms. For these atoms, the charge difference between the Amber charge and the RESP charge was calculated. The charge from GROMOS-96 force

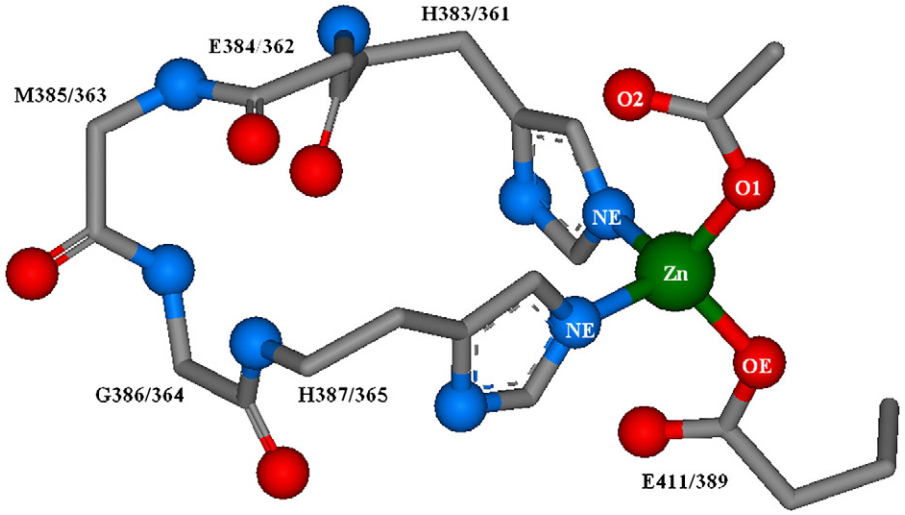

Fig. 1. Model system of the ACE catalytic site for geometry optimization and handling the zinc–inhibitor charge transfer. Residue numbers of the zinc-binding motif refer to the cACE/nACE. Hydrogen atoms are omitted for clarity, carbon atoms are shown as sticks, nitrogen (blue) and oxygen (red) atoms are shown as spheres.

field minus the charge difference to obtain the charges shown in Table S1, were used for MD simulations. Inter-atomic distances and angles are tabulated in Table S2. In Tables S1 and S2, average values are presented, because the charge of the zinc binding atoms, inter-atomic distances and angles for the three inhibitors in the two domains of ACE do not differ much; the maximum standard deviation is 0.3% for those parameters.

2.4. Molecular dynamics simulation

MD simulations have been performed with the GROMACS software package (version 4.05) [24] using the GROMOS-96 force field [25–28]. The enzyme–inhibitor complex was solvated with the explicit SPC water embedded in a truncated octahedral periodic box. The box is generated with the program genbox embedded in Gromacs. The box type is truncated octahedron. The complexes of protein and the inhibitors were solvated with explicit water. The dimensions of the box were based on setting the box edge approx 0.8 nm from the surface of the protein. To neutralize the systems, sodium ions were added by replacing water molecules randomly. The systems were then subjected to steepest descent energy minimization. The temperature of the system was raised from 0 to 300 K in a 15 ps heating phase. Afterwards, a position-restrained simulation for 100 ps was performed. MD simulations were performed at 300 K and 1 bar for 20 ns with a time step of 2 fs, and coordinates were saved every 0.2 ps. Temperature and pressure controls were imposed using a Berendsen-type algorithm [41] with coupling constants of 0.1 ps and 0.5 ps, respectively. The electrostatic interactions were calculated by using the Particle-mesh-Ewald algorithm [41], with an interpolation order of 6 and a grid spacing of 0.12 nm. The cutoff for van der Waals interactions was 1.2 nm. Hydrogen-bonding interactions were monitored using 3.5 Å as the donor–acceptor distance cutoff and 60° as the hydrogen–donor–acceptor angle cutoff. The occupancy of each hydrogen bond was calculated on the basis of the percentage of time that the hydrogen bond existed over the last 10 ns simulation.

3. Results

3.1. Overall conformation of ACE bound to tripeptides

The MD simulations were first tested for the system cACE/lisinopril and nACE/lisinopril. Fig. S2 shows the superpositioning of the structure of MD simulation and that of initial structure. As can be seen, the structure after 20 ns simulation (green) and that of crystal structure (gray) are very well superimposed. For tripeptide/ACE systems, there is very little change in the distances between the zinc and the associating atoms during the course of 20 ns MD simulation (Fig. S3). The results demonstrated that the structure of the zinc and its associating atoms obtained through the QM geometric optimization is stable.

ACE conformation was checked by analyzing the backbone root mean square deviations (RMSD) from the starting crystal structure over the course of the trajectory. RMSD for the complexes of ACE with inhibitors showed that the structures of the four systems equilibrated well after 4 ns of MD simulation (Fig. 2). The radius of gyration (Rg) is an indicator for structural change in a protein [42]. It was calculated to analyze structural changes of ACE, when the inhibitors were bound. The average Rg values throughout the simulation time are 23.2 Å for the cACE complexes, 23.9 Å for nACE/LKP, and 24.0 Å for nACE/IKP (Fig. 3). While for the ACE not bound to the inhibitors, the average Rg values are 23.6 Å for cACE and 24.5 Å for nACE. As seen, upon the binding of the inhibitors, the changes of Rg for cACE and nACE are less than 2.5%. The binding of the inhibitors to ACE does not induce a big change in the solvent accessible surface area (SASA) of the enzyme complexes (Fig. 4). The above results indicate the stability of the overall structure of ACE when the inhibitors are bound.

B-factor is a measurement of disorder; a high B-factor means that a certain group is highly mobile. B-factors were calculated from root-mean square fluctuations of C_α atoms during the course of 20 ns MD trajectory (Fig. S4). Some loop regions between the α-helix and β-sheet exhibit high B-factors, as illustrated with red solid ribbons in Fig. S5. This is consistent with the reported results [19,43]. On the other hand, the regions binding to the inhibitors exhibit lower B-factors.

3.2. Tripeptides in the active site of cACE

The tripeptides (yellow) can interact with the residues of the active site through electrostatic interaction, hydrogen bonds, and hydrophobic interaction (Fig. 5a and b). The most profound structural difference between the two complexes (LKP–cACE and IKP–cACE) centers on the N-terminal residue Leu/Ile of LKP/IKP in the hydrophobic subsite of cACE, comprising Val379, Val380, Phe457, Phe527 and Ala418. These residues have hydrophobic interactions with the side chains of Leu/Ile of LKP/IKP. Both Leu and Ile are an intermediately large, hydrophobic residue. The unique feature of Leu is that its side chain is branched at the Cγ position, while Ile is branched at Cβ. Fig. 5a and b shows that the Leu residue of LKP is held deeper in the hydrophobic subsite than the Ile

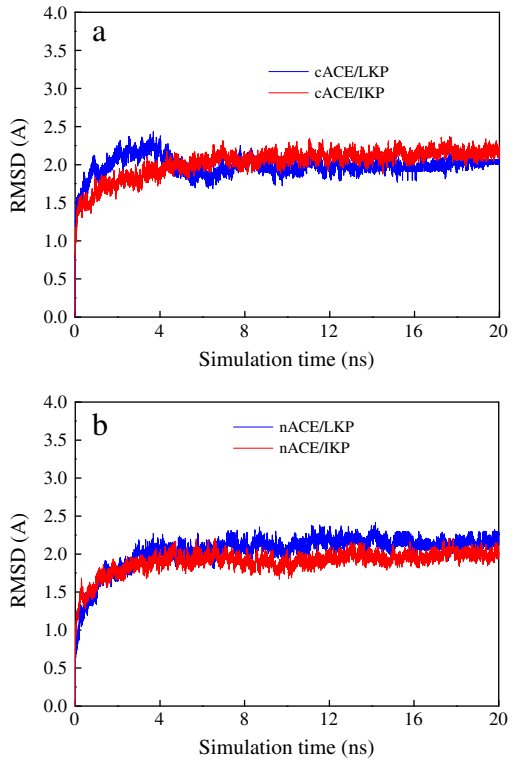

Fig. 2. RMSD as a function of simulation time for the complexes of cACE (a) and nACE (b) with the inhibitors.

residue of IKP. This is reflected from the interactions of the Leu/Ile residue with Val379 (6.16/5.79 Å), Val380 (5.17/4.17), Phe457 (5.57/6.53 Å), Ala418 (6.39/6.91 Å), and Phe527 (6.74/6.78 Å) (Fig. 5a). As seen, the hydrophobic side chain of the Leu residue interacts more favorably with the side chains of Phe457 and Val380. While for the IKP–cACE complex, possibly, because of the configuration of the side chain of Ile and its orientation in the hydrophobic subsite, the side chain of the Ile residue interacts more favorably with the side chain of Val380. As a result, the Ile residue flips away from contacting with Phe457. By contrast, the Leu residue of LKP is well positioned in the hydrophobic subsite. Except for the difference in the hydrophobic interactions, Leu NH_3^+ of LKP makes electrostatic interactions with Asp453 (5.98 Å) and Asp415. In addition, it can form hydrogen bonding interactions with Asp415 OD1 and OD2 and Tyr523 OH. In contrast, Ile NH_3^+ of IKP forms a stronger electrostatic interaction with Asp453 (4.46 Å); however, it cannot form hydrogen bonds with Asp415 OD1 and OD2 and Tyr523 OH.

The above structural analysis indicates that the binding position of Leu of LKP differs from that of Ile of IKP. Fig. 5a and b clearly shows that the binding position of the N-terminal residues influences the accommodation of the middle residue Lys within the active site. Lys NH_3^+ of LKP makes electrostatic interactions with a polar subsite, comprising Asp377, Gln369, Cys352, Ala354, Ser355 and Glu162, and forms hydrogen bonds with Glu162 OE1 and OE2 and Cys352 O. The amide NH of Lys of LKP can form a hydrogen bond with Tyr523 OH. In contrast, in the IKP–cACE complex, Lys NH_3^+ of IKP exhibits electrostatic interactions with Cys352, Ala354, His353, and Lys368, and the Lys NH_3^+ forms hydrogen bonds with Cys352 O, Ala354 O, and Lys368 O.

The Zn^{2+} ion is coordinated by the carboxylate group of the inhibitors. However, due to the different binding position of the N-terminal residues, the distance Zn–Pro O2 (IKP) is larger than the distance Zn–Pro O2 (LKP), indicating a smaller interaction energy between the zinc and the Pro residue of IKP.

3.3. Tripeptides in the active site of nACE

Shown in Fig. 6 is the interaction of tripeptides with the active site of nACE. Similar to the inhibitors in cACE, the carboxylate group of the inhibitors coordinates tightly with the Zn^{2+}. In addition, Pro O2 of the inhibitors makes hydrogen bonds with Tyr501 OH. The N-terminal Leu/Ile of LKP/IKP binds to a hydrophobic subsite of nACE, comprising Phe435, Phe505 and Ala396. The side chains of Leu/Ile of LKP/IKP make hydrophobic interactions with Phe435 (6.28 Å/

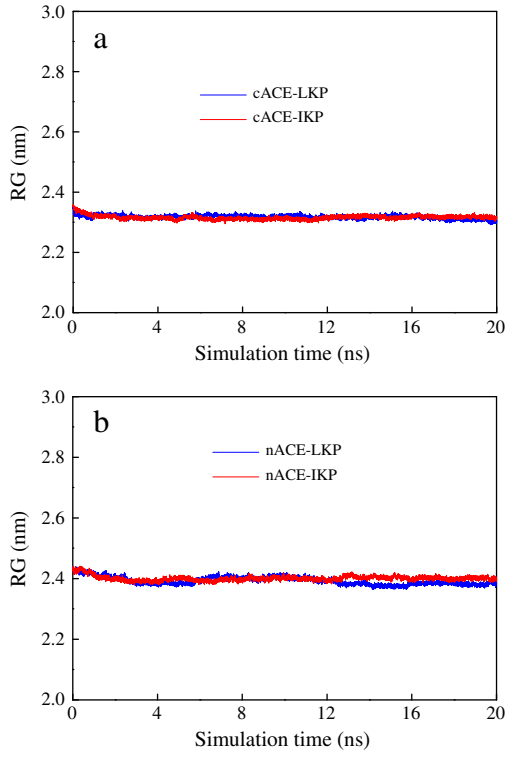

Fig. 3. Radius of gyration (Rg) of the complexes during the course of MD simulation.

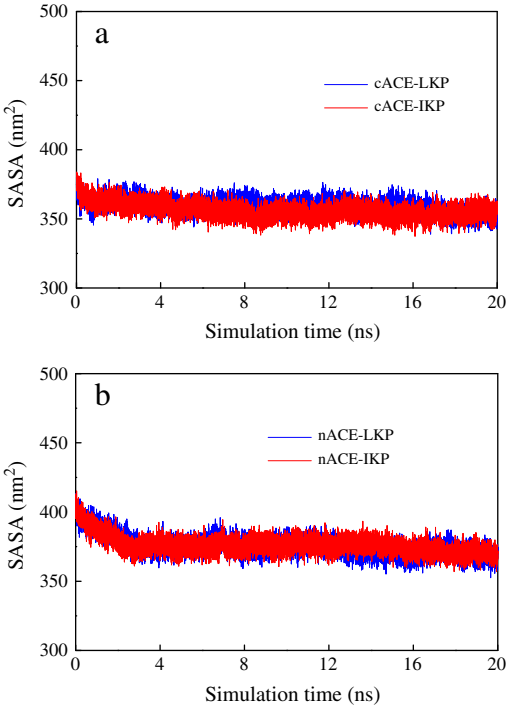

Fig. 4. SASA of the ACE complexes over the course of simulation.

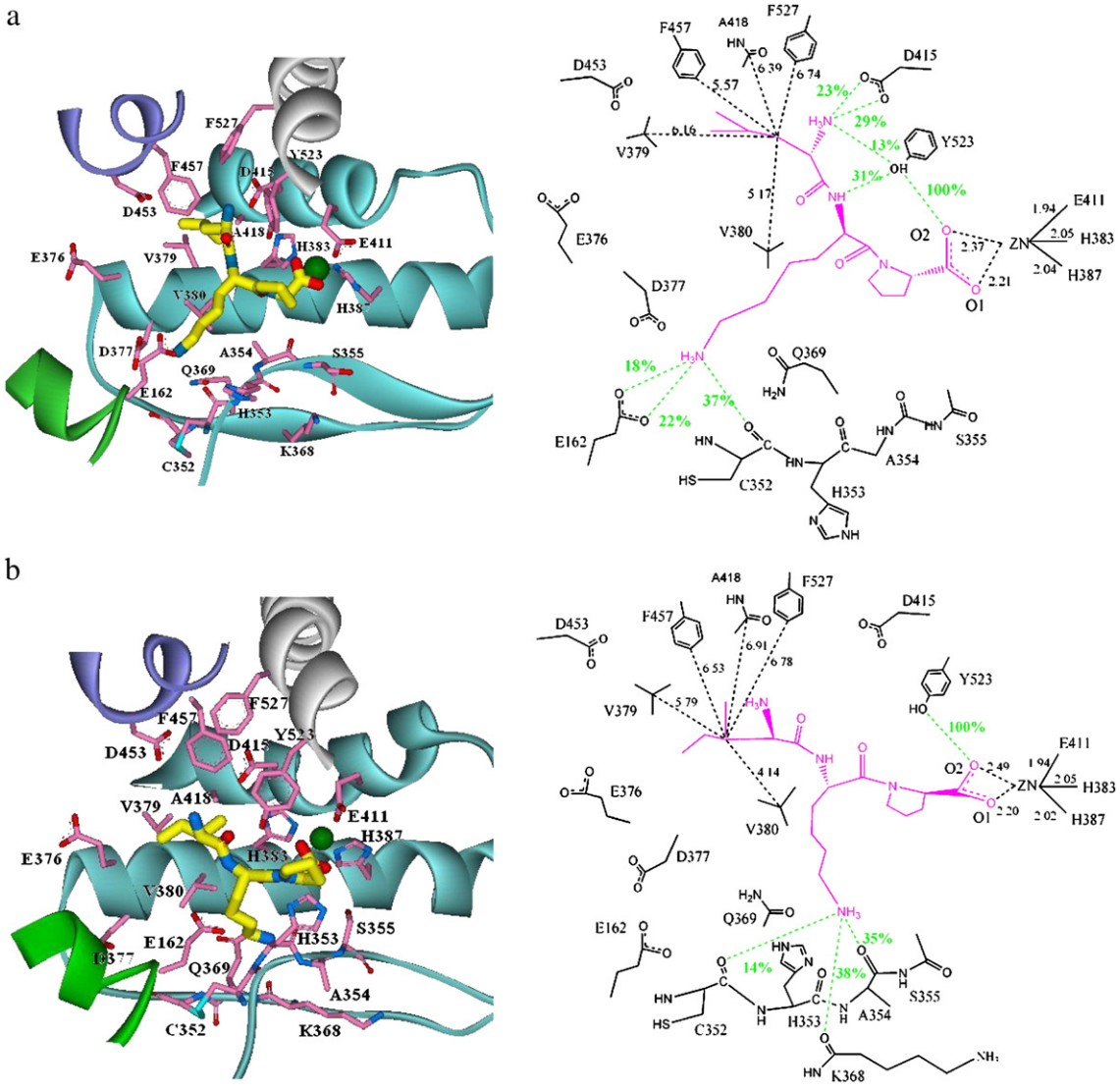

Fig. 5. Tripeptides LKP (a) and IKP (b) binding to the active site of cACE. The configurations are extracted from the MD trajectories of the last ns simulation. Left panel: Overall structures of the C-domain bound to tripeptides (yellow) in the active site. The residues of cACE closely contacting with the inhibitors are drawn as sticks and colored by element: carbon (pink), oxygen (red), nitrogen (blue). The Zn atom is shown as a green sphere. The inhibitors are shown as orange sticks. Right panel: Schematic view of LKP/IKP binding with distances marked in Å. The hydrogen bond occupancies between the atoms connected with dotted green lines are indicated with green numbers. The occupancies and distances (black number) marked in Å are averaged values over the last 10 ns simulations.

6.18 Å), Phe505 (4.69 Å/4.75 Å) and Ala396 (6.38 Å/6.58 Å). As seen, the binding position of the Leu residue is not so different from that of the Ile residue.

Except for the hydrophobic interactions, Leu NH_3^+ of LKP exhibits electrostatic interactions with Asp431, and makes electrostatic and hydrogen bonding interactions with Asp393. Ile NH_3^+ of IKP binds to a polar subsite of nACE, comprising Asp354, Ser357, Ser260 and Asp431. The amide NH of Lys of LKP/IKP makes hydrogen bonds with Thr358 OH. Lys NH_3^+ of LKP exhibits electrostatic interaction with Asp354, Asp140, and Gln355, and can form hydrogen bonding interactions with Asp140 OD1 and OD2. In contrast, Lys NH_3^+ of IKP makes hydrogen bonds with Gln 347 OE and Gln 355 OE.

4. Conclusions and discussion

The interesting structural finding entails the N-terminal residue Leu/Ile of LKP/IKP interacting with a hydrophobic subsite of cACE. Structural analysis reveals that the hydrophobic interaction of the N-terminal residues with the hydrophobic subsite contributes significantly to the difference in binding position between LKP and IKP, and hence further affects the interactions of the middle residue Lys with residues of ACE and the Pro residue with the zinc.

The binding of LKP/IKP in the active site of ACE is influenced by the orientation of Leu/Ile, which is greatly influenced by the interaction with the hydrophobic subsite. Structural analyses of the LKP–cACE and IKP–cACE complexes suggest that, Leu of LKP fits snugly in the vicinity of the hydrophobic subsite of cACE, where the Leu residue forms extensive hydrophobic, electrostatic, and hydrogen bonding interactions with the residues of cACE. These interactions play an important role in stabilizing LKP in the complex, thus contributing to high specificity LKP binding to cACE. While, the mutation of Leu to Ile reduces the interaction energy of the tripeptide with cACE (Table S3), underscoring the importance of the interactions of N-terminus with the hydrophobic subsite.

To further explain the results, we compared the residues between the N- and C-domains of somatic human ACE contacting with the inhibitors (Table S4). 8 of the 14 residues are strictly conserved between cACE and nACE. In the C-domain, Val379 and Val380 are the important residues of the hydrophobic subsite interacting with the side chains of Leu/Ile of LKP/IKP. While the N-domain has Ser357

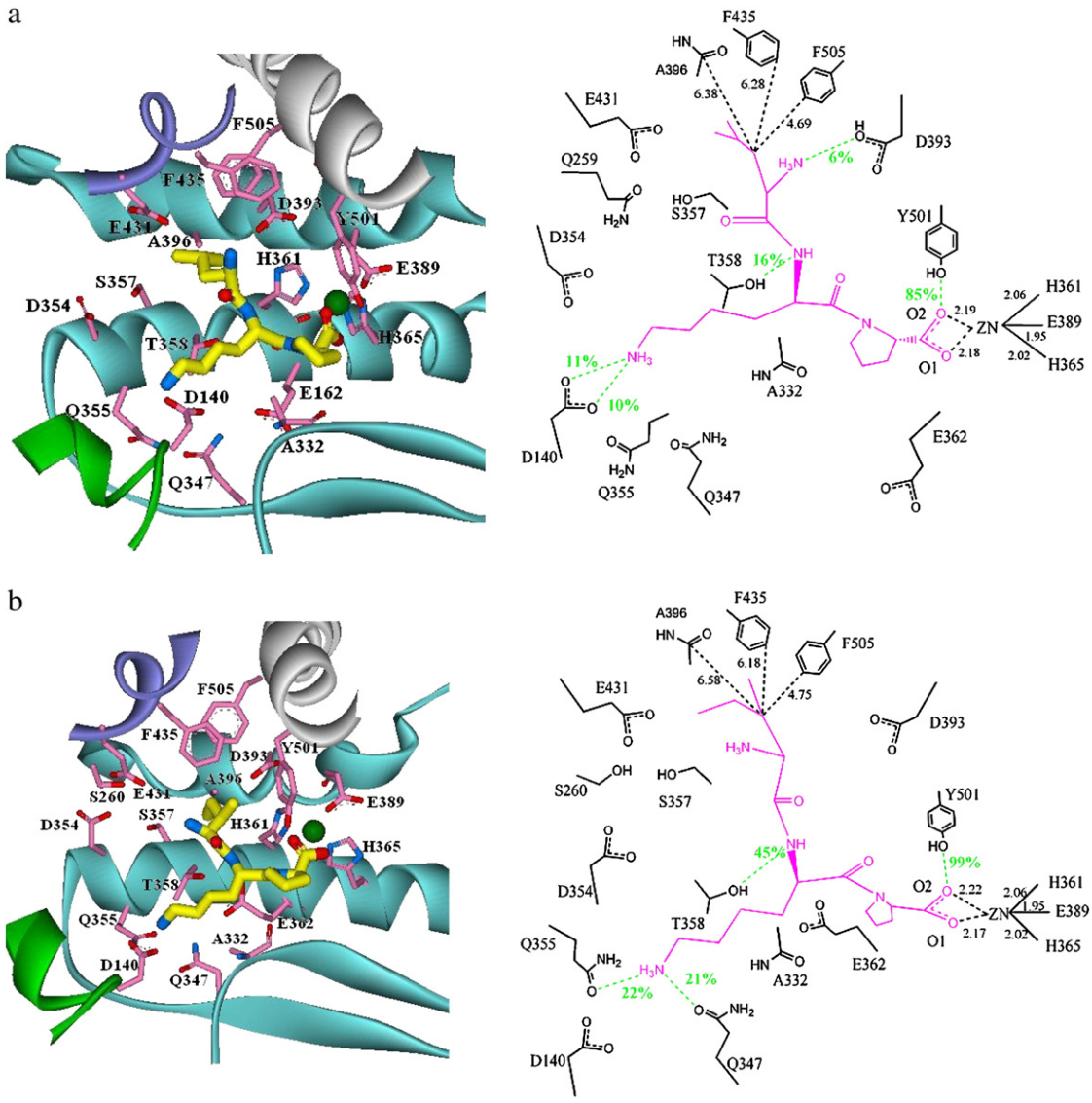

Fig. 6. Tripeptides LKP (a) and IKP (b) binding to the active site of nACE. The configurations are extracted from the MD trajectories of the last ns simulation. Left panel. Overall structures of the N-domain bound to tripeptides (yellow) in the active site. The residues of nACE closely contacting with the inhibitors are drawn as sticks and colored by element: carbon (pink), oxygen (red), nitrogen (blue). The Zn atom is shown as a green sphere. Right panel: Schematic view of LKP/IKP binding with distances marked in Å. The hydrogen bond occupancies between the atoms connected with dotted green lines are indicated with green numbers. The occupancies and distances (black number) marked in Å are averaged values over the last 10 ns simulations.

and Thr358 at equivalent positions [44]; they are polar residues, making weak interactions with the side chain of Leu/Ile. Both the side chains of Leu and Ile of the inhibitors make hydrophobic interactions with Phe435, Phe505, and Ala396. The distances indicated in Fig. 6b (right panel) imply that there is no preferential hydrophobic interactions between the Leu and Ile residues, indicative of the binding position of Leu of LKP that is not so different from that of Ile of IKP in nACE. On the other hand, the residue Thr358 has a hydrogen bonding interaction with Lys N of LKP/IKP. This hydrogen bonding interaction contributes to the restriction of the movement of backbone of LKP and IKP.

Both the structural analysis and interaction energies (Table S3) indicate that, LKP exhibits higher inhibitory potency than IKP for the C-domain; while the two tripeptides have almost the same inhibitory potency for N-domain. ACE possesses two independent active sites, and the C-/N-domain independently binds an inhibitor molecule [45]. The significant difference in the IC_{50} values between LKP and IKP is possibly because of their different potencies for the C-domain. The simulation work unveils the molecular determinants for the high affinity LKP binding to cACE. The identified hydrophobic subsite in cACE can be exploited to fine-tune the specificity of peptide inhibitors. The results are expected to be valuable in structure-based rational design of different classes of ACE inhibitors for potential therapeutic use.

Acknowledgments

This work was supported by the National Science Foundation of China (21076018, 21176025) and the National Basic Research Program of China (2011CB200905).

Appendix A. Supplementary data

Supplementary data to this article can be found online at http://dx.doi.org/10.1016/j.bpc.2012.05.002.

References

[1] C.S. Anthony, H.R. Corradi, S.L. Schwager, U.P. Redelinghuys, D. Georgiadis, V. Dive, K.R. Acharya, E.D. Sturrock, The N domain of human angiotensin-I-converting enzyme: the role of N-glycosylation and the crystal structure in complex with an N domain-specific phosphinic inhibitor, RXP407, Journal of Biological Chemistry 285 (2010) 35685–35693.

[2] X. Liu, C.O.C. Bellamy, B.A. Bailey, L.J. Mullins, D.R. Dunbar, C.J. Kenyon, G. Brooker, S. Kantachuvesiri, K. Maratou, A. Ashek, A.F. Clark, S. Fleming, J.J. Mullins, Angiotensin-converting enzyme is a modifier of hypertensive end organ damage, Journal of Biological Chemistry 284 (2009) 15564–15572.

[3] K. Zou, T. Maeda, A. Watanabe, J. Liu, S. Liu, R. Oba, Y.I. Satoh, H. Komano, M. Michikawa, Aβ-42-to-Aβ-40 and angiotensin-converting activities in different domains of angiotensin-converting enzyme, Journal of Biological Chemistry 284 (2009) 31914–31920.

[4] R. Natesh, S.L.U. Schwager, E.D. Sturrock, K. Ravi Acharya, Crystal structure of the human angiotensin-converting enzyme–lisinopril complex, Nature 421 (2003) 551–554.

[5] Z.L. Woodman, S.L. Schwager, P. Redelinghuys, A.J. Chubb, E.L. van der Merwe, M.R. Ehlers, E.D. Sturrock, Homologous substitution of ACE C-domain regions with N-domain sequences: effect on processing, shedding, and catalytic properties, Journal of Biological Chemistry 387 (2006) 1043–1051.

[6] H.R. Corradi, I. Chitapi, B.T. Sewell, D. Georgiadis, V. Dive, E.D. Sturrock, K.R. Acharya, The structure of testis angiotensin-converting enzyme in complex with the C domain-specific inhibitor RXPA380, Biochemistry 46 (2007) 5473–5478.

[7] J.M. Watermeyer, W.L. Kroger, H.G. O'Neill, B.T. Sewell, E.D. Sturrock, Probing the basis of domain-dependent inhibition using novel ketone inhibitors of angiotensin-converting enzyme, Biochemistry 47 (2008) 5942–5950.

[8] H.R. Corradi, S.L.U. Schwager, A.T. Nchinda, E.D. Sturrock, K.R. Acharya, Crystal structure of the N domain of human somatic angiotensin I-converting enzyme provides a structural basis for domain-specific inhibitor design, Journal of Molecular Biology 357 (2006) 964–974.

[9] T.F.T. Antonios, G.A. Macgregor, Angiotensin-converting enzyme-inhibitors in hypertension — potential problems, Journal of Hypertension 1 (1995) S11–S16.

[10] L. Vercruysse, J. Van Camp, G. Smagghe, ACE inhibitory peptides derived from enzymatic hydrolysates of animal muscle protein: a review, Journal of Agricultural and Food Chemistry 53 (2005) 8106–8115.

[11] M. Martin, A. Wellner, I. Ossowski, T. Henle, Identification and quantification of inhibitors for angiotensin-converting enzyme in hypoallergenic infant milk formulas, Journal of Agricultural and Food Chemistry 56 (2008) 6333–6338.

[12] H. Li, R.E. Aluko, Identification and inhibitory properties of multifunctional peptides from pea protein hydrolysate, Journal of Agricultural and Food Chemistry 58 (2010) 11471–11476.

[13] R.J. FitzGerald, H. Meisel, Milk protein-derived peptide inhibitors of angiotensin-I-converting enzyme, British Journal of Nutrition 84 (2000) S33–S37.

[14] S. Makinen, J. Kelloniemi, A. Pihlanto, K. Makinen, H. Korhonen, A. Hopia, J.P.T. Valkonen, Inhibition of angiotensin converting enzyme I caused by autolysis of potato proteins by enzymatic activities confined to different parts of the potato tuber, Journal of Agricultural and Food Chemistry 56 (2008) 9875–9883.

[15] T. Nakamura, A. Yoshida, N. Komatsuzaki, T. Kawasumi, J. Shima, Isolation and characterization of a low molecular weight peptide contained in sourdough, Journal of Agricultural and Food Chemistry 55 (2007) 4871–4876.

[16] M. Terashima, T. Baba, N. Ikemoto, M. Katayama, T. Morimoto, S. Matsumura, Novel angiotensin-converting enzyme (ACE) inhibitory peptides derived from boneless chicken leg meat, Journal of Agricultural and Food Chemistry 58 (2010) 7432–7436.

[17] M. Liu, M. Pazgier, C. Li, W. Yuan, C. Li, W. Lu, A left-handed solution to peptide inhibition of the p53–MDM2 interaction, Angewandte Chemie (International Ed. in English) 49 (2010) 3649–3652.

[18] H. Fujita, K. Yokoyama, M. Yoshikawa, Classification and antihypertensive activity of angiotensin I-converting enzyme inhibitory peptides derived from food proteins, Journal of Food Science 65 (2000) 564–569.

[19] A. Papakyriakou, G.A. Spyroulias, E.D. Sturrock, E. Manessi-Zoupa, P. Cordopatis, Simulated interactions between angiotensin-converting enzyme and substrate gonadotropin-releasing hormone: novel insights into domain selectivity, Biochemistry 46 (2007) 8753–8765.

[20] N. Dimitropoulos, A. Papakyriakou, G.A. Dalkas, E.D. Sturrock, G.A. Spyroulias, A computational approach to the study of the binding mode of dual ACE/NEP inhibitors, Journal of Chemical Information and Modeling 50 (2010) 388–396.

[21] X. Wang, S. Wu, D. Xu, D. Xie, H. Guo, Inhibitor and substrate binding by angiotensin-converting enzyme: quantum mechanical/molecular mechanical molecular dynamics studies, Journal of Chemical Information and Modeling 51 (2011) 1074–1082.

[22] N. Guex, M.C. Peitsch, SWISS-MODEL and the Swiss-PdbViewer: an environment for comparative protein modeling, Electrophoresis 18 (1997) 2714–2723.

[23] J.C. Gordon, J.B. Myers, T. Folta, V. Shoja, L.S. Heath, A. Onufriev, H++: a server for estimating pKas and adding missing hydrogens to macromolecules, Nucleic Acids Research 23 (2005) 368–371.

[24] B. Hess, GROMACS 4: algorithms for highly efficient, load-balanced, and scalable molecular simulation, Journal of Chemical Theory and Computation 4 (2008) 435–447.

[25] W.F. van Gunsteren, H.J.C. Berendsen, Gromos-87 manual, Biomos BV Nijenborgh 4, 9747 AG Groningen, The Netherlands, 1987.

[26] M. Manna, C. Mukhopadhyay, Molecular dynamics simulations of the interactions of kinin peptides with an anionic POPG bilayer, Langmuir 27 (2011) 3713–3722.

[27] M.A. Barhoover, T. Orban, D.O. Beck, M.A. Bukys, M. Kalafatis, Contribution of amino acid region 334–335 from factor Va heavy chain to the catalytic efficiency of prothrombinase, Biochemistry 47 (2008) 6840–6850.

[28] M. Pasi, L. Riccardi, P. Fantucci, L. De Gioia, E. Papaleo, Dynamic properties of a psychrophilic r-amylase in comparison with a mesophilic homologue, The Journal of Physical Chemistry. B 113 (2009) 13585–13595.

[29] G.M. Morris, D.S. Goodsell, R.S. Halliday, R. Huey, W.E. Hart, R.K. Belew, A.J. Olson, Automated docking using a Lamarckian genetic algorithm and an empirical binding free energy function, Journal of Computational Chemistry 19 (1998) 1639–1662.

[30] M.A. Ondetti, B. Rubin, D.W. Cushman, Design of specific inhibitors of angiotensin-converting enzyme: new class of orally active antihypertensive agents, Science 196 (1977) 441–444.

[31] A.A. Patchett, E. Harris, E.W. Tristam, M.J. Wyvratt, M.T. Wu, D. Taub, E.R. Peterson, T.J. Ikeler, J. Ten Broeke, L.G. Payne, D.L. Ondeyka, E.D. Thorsett, W.J. Greenlee, N.S. Lohr, R.D. Hoffsommer, H. Joshua, W.V. Ruyle, J.W. Rothrock, S.D. Aster, A.L. Maycock, F.M. Robinson, R. Hirschmann, C.S. Sweet, E.H. Ulm, D.M. Gross, T.C. Vassil, C.A. Stone, A new class of angiotensin-converting enzyme inhibitors, Nature 288 (1980) 280–283.

[32] X. Hu, W.H. Shelver, Docking studies of matrix metalloproteinase inhibitors: zinc parameter optimization to improve the binding free energy prediction, Journal of Molecular Graphics and Modelling 22 (2003) 115–126.

[33] O.A. Donini, P.A. Kollman, Calculation and prediction of binding free energies for the matrix metalloproteinases, Journal of Medicinal Chemistry 43 (2000) 4180–4188.

[34] Y. Pang, K. Xu, J. Yazal, F.G. Prendergast, Successful molecular dynamics simulation of the zinc-bound farnesyltransferase using the cationic dummy atom approach, Protein Science 9 (2000) 1857–1865.

[35] R.H. Stote, M. Karplus, Zinc binding in proteins and solution: a simple but accurate nonbonded representation, Proteins 23 (1995) 12–31.

[36] S.C. Hoops, K.W. Anderson, K.M. Merz, Force field design for metalloproteins, Journal of the American Chemical Society 113 (1991) 8262–8270.

[37] T.J. Hou, W. Zhang, X.J. Xu, Binding affinities for a series of selective inhibitors of gelatinase-A using molecular dynamics with a linear interaction energy approach, The Journal of Physical Chemistry. B 105 (2001) 5304–5315.

[38] S. Toba, K.V. Damodaran, K.M. Jr Merz, Binding preferences of hydroxamate inhibitors of the matrix metalloproteinase human fibroblast collagenase, Journal of Medicinal Chemistry 42 (1999) 1225–1234.

[39] M.J. Frisch, G.W. Trucks, H.B. Schlegel, G.E. Scuseria, M.A. Robb, J.R. Cheeseman, V.G. Zakrzewski, J.A. Montgomery, R.E. Jr Stratmann, J.C. Burant, S. Dapprich, J.M. Millam, A.D. Daniels, K.N. Kudin, M.C. Strain, O. Farkas, J. Tomasi, V. Barone, M. Cossi, R. Cammi, B. Mennucci, C. Pomelli, C. Adamo, S. Clifford, J. Ochterski, G.A. Petersson, P.Y. Ayala, Q. Cui, K. Morokuma, D.K. Malick, A.D. Rabuck, K. Raghavachari, J.B. Foresman, J. Cioslowski, J.V. Ortiz, B.B. Stefanov, G. Liu, A. Liashenko, P. Piskorz, I. Komaromi, R. Gomperts, R.L. Martin, D.J. Fox, T. Keith, M.A. Al-Laham, C.Y. Peng, A. Nanayakkara, C. Gonzalez, M. Challacombe, P.M.W. Gill, B.G. Johnson, W. Chen, M.W. Wong, J.L. Andres, M. Head-Gordon, E.S. Replogle, J.A. Pople, Gaussian 98, Revision A.9, Gaussian, Inc., Pittsburgh, PA, 1998.

[40] C.I. Bayly, P. Cieplak, W.D. Cornell, P.A. Kollman, A well-behaved electrostatic potential based method using charge restraints for deriving atomic charges: the RESP model, Journal of Physical Chemistry 97 (1993) 10269–10280.

[41] H.J.C. Berendsen, J.P.M. Postma, A. DiNola, J.R. Haak, Molecular dynamics with coupling to an external bath, Journal of Chemical Physics 81 (1984) 3684–3690.

[42] U. Essmann, L. Perera, M.L. Berkowitz, T. Darden, H. Lee, L.G.A. Pedersen Smooth, Particle mesh Ewald potential, Journal of Chemical Physics 103 (1995) 8577–8592.

[43] J.M. Watermeyer, B.T. Sewell, S.L. Schwager, R. Natesh, H.R. Corradi, K.R. Acharya, E.D. Sturrock, Structure of testis ACE glycosylation mutants and evidence for conserved domain movement, Biochemistry 45 (2006) 12654–12663.

[44] M. Akif, D. Georgiadis, A. Mahajan, V. Dive, E.D. Sturrock, R.E. Isaac, K.R. Acharya, High-resolution crystal structures of *Drosophila melanogaster* angiotensin-converting enzyme in complex with novel inhibitors and antihypertensive drugs, Journal of Molecular Biology 400 (2010) 502–517.

[45] L. Wei, E. Clauser, F. Alhenc-Gelas, P. Corvol, The two homologous domains of human angiotensin I-converting enzyme interact differently with competitive inhibitors, Journal of Biological Chemistry 267 (1992) 13398–13405.